Since January 2020 Elsevier has created a COVID-19 resource centre with free information in English and Mandarin on the novel coronavirus COVID-19. The COVID-19 resource centre is hosted on Elsevier Connect, the company's public news and information website.

High sensitivity graphene based health sensor with self-warning function

Lu-Qi Tao, Chenwei Gao, Guanya Wang, Hao Sun, Liang-Yan Guo, Tian-Ling Ren

PII: S0266-3538(23)00216-6

DOI: https://doi.org/10.1016/j.compscitech.2023.110123

Reference: CSTE 110123

To appear in: *Composites Science and Technology*

Received Date: 3 March 2023

Revised Date: 1 May 2023

Accepted Date: 16 June 2023

Please cite this article as: Tao L-Q, Gao C, Wang G, Sun H, Guo L-Y, Ren T-L, High sensitivity graphene based health sensor with self-warning function, *Composites Science and Technology* (2023), doi: https://doi.org/10.1016/j.compscitech.2023.110123.

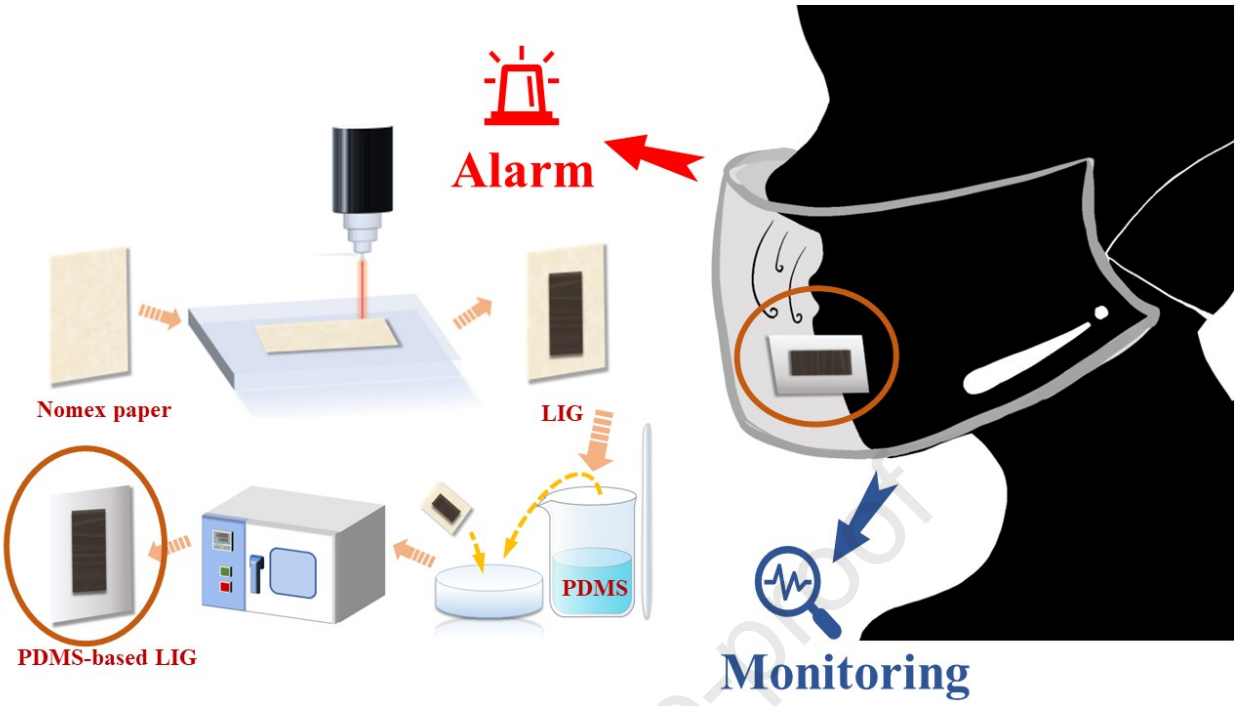

High Sensitivity Graphene Based Health Sensor with Self-warning Function

Lu-Qi Tao [a], Chenwei Gao [b], Guanya Wang [b], Hao Sun [b], Liang-Yan Guo [b,*], Tian-Ling Ren [c,*]

[a] Beijing Engineering Research Center of Industrial Spectrum Imaging, School of Automation and Electrical Engineering, University of Science and Technology Beijing, Beijing 100083, China

[b] National Key Laboratory of Power Transmission Equipment Technology, School of Electrical Engineering, Chongqing University, Chongqing 400044, China.

[c] Institute of Microelectronics and Beijing National Research Center for Information Science and Technology (BNRist), Tsinghua University, Beijing 100084, China.

* Corresponding author: Liang-Yan Guo (Tel: +86-15938171920; Email: guoliangyan@cqu.edu.cn);

Tian-Ling Ren (Tel: +86-10-62798569; Email: RenTL@tsinghua.edu.cn).

Abstract

In order to reduce the damage to people's health from diseases that attack the respiratory system such as COVID-19, asthma, and pneumonia, it is desired that patients' breathing can be monitored and alerted in real-time. The emergence of wearable health detection sensing devices has provided a relatively good response to this problem. However, there are still problems such as complex structure and poor performance. This paper introduces a laser-induced graphene (LIG) device that is attached to PDMS. The LIG is produced by laser irradiation of Nomex and subsequently transferred and attached to the PDMS. After being tested, it has demonstrated high sensitivity, stable tensile performance, good acoustic performance, excellent thermal stability, and other favorable properties. Notably, its gauge factor (GF) value can reach 721.67, which is quite impressive. Additionally, it is capable of emitting an alarm sound with an SPL close to 60 dB when receiving signals within the range of 5 - 20 kHz. The device realizes mechanical sensing and acoustic functions in one chip, and has a high application value in applications that need to combine sensing and early warning.

Keywords: Laser-induced graphene, Tensile strain sensor, Health monitoring, Wearable devices, Flexible electronics.

1. Introduction

In modern society, health has become an issue of close concern for everyone. COVID-19 has a more serious impact on the breathing of patients (including the sequelae of cured patients) and is even the culprit of death [1]. It cannot be overlooked that the absence of timely alarm measures in case of sudden onset is one of the fatal causes of high mortality. To solve this problem, a variety of sensing devices have been intensively researched and used for health monitoring as assistive devices for real-time monitoring of a patient's physical status [2]-[4]. These wearable devices have the following drawbacks: firstly, their health monitoring and alarm functions require wireless transmission modules such as Bluetooth, which is highly likely to cause delayed signal transmission and delayed alarms, causing patients to miss the best opportunity for treatment. In addition, these wearable devices are composed of various detection and alarm components to achieve multi-functional integration, including sensors, vibration motors, buzzers, and so on [5], [6]. A sensing device with the integration of an alarm function is urgently needed. Besides, existing research on sensing devices oriented toward health detection has gradually shifted from single-parameter detection to integrated and multifunctional implementations [7]. The desired sensors should have various characteristics such as user-friendliness, accessibility, and high flexibility, which can be broadly applied in medical and healthcare. So finding suitable sensing materials and designing functionally integrated and efficient sensing devices have become the focus of current research [8]. In addition, such sensing technologies that can integrate mechanical sensing and alarm functions can be used not only in health monitoring devices but also in some applications where

behaviors are required to cause sound, such as respiration detection, gait detection, motion recognition, human-machine interaction (HMI), and so on [9]-[14].

The selection of sensing materials is one of the main challenges to achieving wearable sensors with both a good gauge factor (GF) as well as an alarm function, to achieve multifunctional integration. And after various studies, graphene-based materials have been found to have many beneficial properties for biomonitoring and are highly advantageous in sensing various biochemical and biophysical signals. As one of the most promising carbon nanomaterials, graphene and its derivatives have been used as the most popular materials in various sensor materials due to their special physicochemical and structural properties. Graphene has various superior properties such as large surface area, high electron mobility, high thermal conductivity, good mechanical strength, good biocompatibility, and excellent chemical stability [14], [12]. Its structure and properties make graphene and its derivatives and suitability for use in devices that need sensitive and fast response. There are many methods in the preparation of graphene, such as mechanical exfoliation, chemical oxidation, crystal epitaxial growth, chemical vapor deposition, organic synthesis, and carbon nanotube exfoliation [13]-[17]. In 2014, Lin and his colleagues first discovered laser-induced graphene (LIG), LIG is produced by direct irradiation of carbonaceous precursors at a very fast rate, which can behave like a three-dimensional porous structure without subsequent processing, and its physical and electrical properties can be easily controlled by changing the relevant parameters of the laser and the substrate and other factors [18]-[20]. Due to its advantages of simple preparation, easy synthesis, low cost, environmental friendliness, and mass production, graphene, and its derivatives LIG have been widely used in various devices, such as supercapacitors, heaters, and so on. This is reflected in various fields such as wearable devices [21]-[25]. The choice of substrate is also very significant in the process of LIG preparation.

For the commonly used polyimide (PI), epoxy resin, and other materials, the stretching ability of these substrates is very limited, and it's convenient to obtain LIG from the PI substrate and compromise the performance of the device [19]. In the work of Chen and his teammates, the performances of LIG devices (also called E-skins) with various patterns on PI substrates have been investigated in detail, and their applications have been reasonably conceived and tested. However, it can be noted that the tensile properties of this "E-skin" are limited and the sensitivity is restricted. To solve this problem, Nomex paper is a common flexible insulating polymer with excellent mechanical strength, good acoustic properties, and a flatter and smoother surface than PI, making it more suitable for integration into wearable devices. In addition, Nomex is also cheaper and can be converted into carbon material by specific methods. Given the three-dimensional porous structure of graphene, Nomex can be chosen as the substrate to obtain LIG and transferred to elastic polydimethylsiloxane (PDMS) substrate, which results in a material with high tensile strain properties [26]. In particular, it can be noted that most of the existing studies have only focused on the mechanical properties of these LIG devices, and there have been few studies on LIG devices printed on Nomex, whereas the transferred LIG devices have better mechanical properties and also perform well in terms of acoustic and thermal stability. Wang then experimentally tested the performance of the LIG flexible integrated heater which will provide us with new considerations for their integration and create a feasible way to implement them in various sensing devices that need to integrate with a wide range of functions [27], [28].

In this paper, we use different power lasers to create rectangular LIGs., transferred them to PDMS with better tensile properties, and tested their mechanical and acoustic properties. We printed rectangular LIG patterns on Nomex using a laser with 3.6 – 5.0 W and 100 mm/s as parameters and transferred them to PDMS films. The surface

structure was characterized using scanning electron

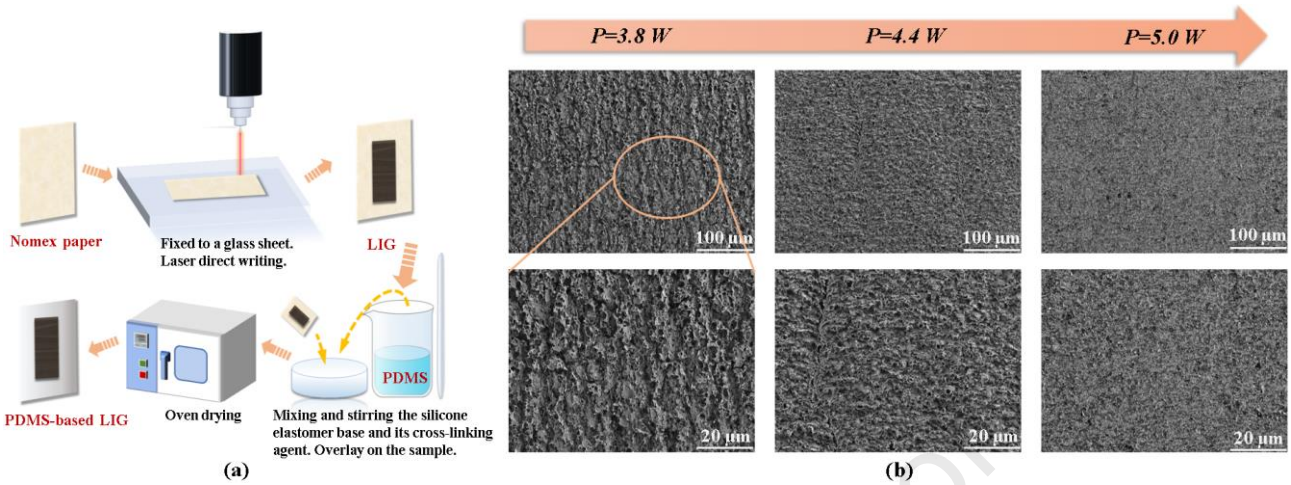

Fig. 1. (a) Schematic diagram of the sample preparation process. (b) Fabrication and characterization of the produced LIG, the SEM images show the porous morphology of LIG. From left to right, the laser power is 3.8 W, 4.4 W, and 5.0 W respectively.

microscopy (SEM). In addition, we measured its mechanical properties including resistance change under cyclic stretch-release, the response rate to external stress, and GF value using a universal testing machine; its acoustic properties such as SPL value were measured using a set of acoustic measurement instruments, and the thermal stability of the sample was also investigated using a heating table. In addition, we designed a verification experiment for respiratory monitoring to confirm the application of the prepared LIG devices in wearable health monitoring devices.

2. Material and methods

2.1 Materials

In this experiment, Nomex paper (T410, DuPont) with a thickness of 130 μm was used. Absolute ethanol was used to flush the Nomex paper. Nomex paper will be applied to laser printing to produce LIG. PDMS, containing SYLGARD 184 silicone elastomer matrix and its curing agent.

2.2 Fabrication of PDMS-based LIG Devices with Different Power and Characterization

The PDMS-based LIG device was prepared according to the flowchart shown in Fig. 1(a) by the

following method: First, cut a square Nomex paper of suitable size, adhered the four sides of the paper with transparent tape, and fixed it flatly on a glass sheet cleaned with anhydrous ethanol. The prepared Nomex paper was put into the laser printer and the relevant parameters for printing (printing speed was 100mm/s, printing interval was 0.01mm) were programmed in advance in the computer software. Irradiation was conducted by a commercial carbon dioxide (CO_2) laser engraving machine (E- 5030, Cixi Jinyue Laser Technology). in which the laser wavelength was 10.6 mm and the beam size was 150 mm. The writing spacing was fixed at 20 mm.

In this experiment, the laser power was set as the gradient variable and the effect of different laser powers on the performance of LIG devices is investigated. The power range that can be transferred smoothly is 3.6 – 5.0 W during the experiment. Six 16 mm * 24 mm rectangular LIG patterns of the same size were printed on the square Nomex paper at uniform intervals, and the printed papers were fixed in the square Petri dishes with double-sided adhesive, which must guarantee that there were no bubbles or protrusions between the films and the bottom of the Petri dishes.

Subsequently, the silicone elastomer base and its cross-linking agent were used to produce a PDMS substrate with better performance (a 12:1 mass ratio was tested to be optimal): The mixture was stirred and mixed, and the air bubbles were sufficiently removed by pouring it into a square Petri dish to cover the surface of the Nomex paper evenly. Immediately afterward, the Petri dish was placed in a hot air oven to dry, taking care to keep the bottom of the Petri dish level to prevent it from being skewed and causing unevenness in the cured PDMS film. After 2 - 4 hours, the Petri dish was removed and the mixture is found to have formed a cured PDMS film on the surface of the LIG. Removing it gently, the LIG came off the Nomex paper nicely and transferred and adhered to the PDMS. The uncovered PDMS was cut according to the shape of the printed LIG and a gap was left around it for subsequent operations. The PDMS-based LIG

instrument for experimental testing was completed by gluing copper wires on both sides of the resulting LIG device and applying silver paste as the conductive medium in its center. The surface morphology of these LIG devices was characterized by scanning electron microscopy (SEM) (The Czech Republic: the TESCAN MIRA LMS).

2.3 The Mechanical and Acoustical Testing of the LIG Devices

The testing of mechanical properties will be done by a universal testing machine and a digital source meter. The universal testing machine, digital source meter, and computer will be connected and the fabricated LIG device will be clamped to the universal testing machine in an appropriate position to ensure that the conductive part of the LIG can be exposed just right. Set the parameters of the tensile strain or cycle of the universal testing machine on the computer using the auxiliary software, and similarly record and observe the resistance and current changes of the measured sample during the tensile and compression process in the computer software. The different strain was applied to the samples by a universal testing machine (ETM-503B, Shenzhen Wance Testing Machine Co., Ltd.). And the resistance changes of samples during the stretching/releasing process were recorded by a digital source meter (Keithley 2450).

The testing of acoustical properties will be done by a set of acoustic measurement instruments, which includes a standard microphone, a function generator, and a dynamic signal analyzer. The sample was applied an AC sinusoidal signal with a different frequency from 200 Hz to 20 kHz by an arbitrary function signal generator (FY 3200S, Feel Tech). Under the applied AC voltage. A standard microphone (MNP 21, SKC), which had a high sensitivity of 51.9 mV Pa^{-1}, was used to capture the sound emitted from the E-skin alarm and convert it into electrical signal. The dynamic signal analyzer (Q401, SKC) was used to analyze the electrical signal and transform it into a frequency domain to record the SPL values of the tested sample at

different frequencies. The heating of the sample will be completed by the heating table (JW-350).

2.4 The Verification in Health Monitoring and Alarm of the LIG Devices

The device that simulates health monitoring, as well as an alarm function, will consist of a mask with LIG devices attached, a microcontroller (micro control unit), and a signal generator. It has two modes of operation: monitoring and alerting. In general, the system works in monitoring mode. Whenever abnormal respiration of the subject wearing the mask is detected (it also could be seen as when the strain value of the device continues to be a small value) for a certain period of time, the microcontroller will control the signal generator to apply AC voltage to the device to give an alarm and switch to the alarm mode.

3. Results and discussion

3.1 The Preparation and Characterization of the LIG Devices

As shown in **Fig. 1(b)**, from the low-resolution images, it can be observed that the LIG on PDMS shows a curled and folded lamellar structure with LIG sheets embedded in the PDMS. As the laser power increases, the structure is more porous and looser, and the LIG lamellae on PDMS are rougher, denser, and gradually cover the PDMS sheet. After

the image magnification increases, it can be observed more clearly that the exposed PDMS gradually becomes less, indicating that the stronger the photothermal effect is, the thicker the generated LIG sheet layer is. This is because the high temperature caused by the laser makes the C=O, C=O, and C=N bonds in the Nomex film break more easily. And the microporous structure is formed because the high local heating energy generated by the CO_2 laser causes the gas products to be released rapidly.

3.2 The Mechanical Performance of the LIG Devices

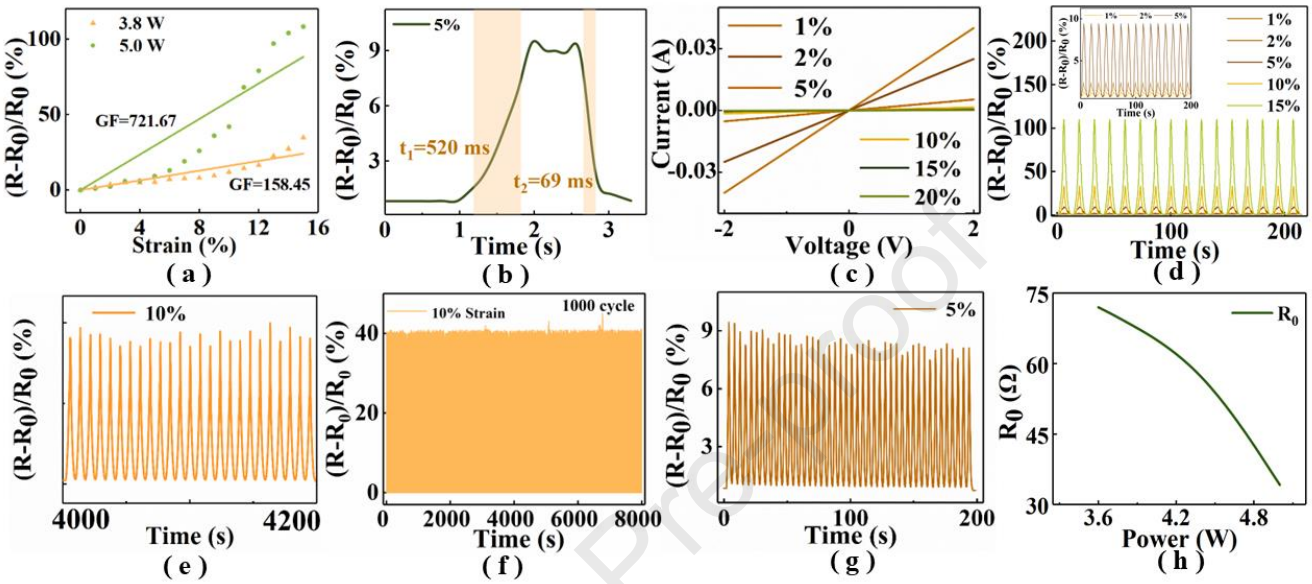

Fig. 2. Strain-responsive performances of the LIG sample. (a) the strain values of the sample at the tensile stresses of 0-15 % and the corresponding GF value. (b) The response time and the recovery time of the sample to a stress of 5 % at the velocity of 500 m/s. (c) The I−V curves of the sample with strain. (d) Comparison of the cyclic response for the sample under different strains of 1, 2, 5, 10, and 15 %. (e) The relative resistance of the sample at 5 % repeated tensile-release cyclic strain. (f) Cycling performance of the sample for 1000 cycling tests under cyclic tensile loading and unloading of 10 %. (g) Magnified picture of the cycling test in (f), showing the stability of the sample. (h) Initial resistance change curve of LIG samples at different laser power.

Fig. 2. (a) shows the strain values of the fabricated sample at smaller tensile stresses (0 – 15 %). The change in performance under stress is represented by its relative resistance change $(R - R_0)/R_0$ in the equation indicates the initial resistance value of the sample when no stress is applied, and R indicates the resistance value reached by the sample under different stresses. It can be visually observed from the figure that the relative resistance change rate of the sample increases significantly monotonically with the increase of the applied stress. When the stretching rate reaches 15 %, the relative resistance change value can reach 108.25, a greatly enhanced value compared to that without the use of PDMS

substrate. Besides, after using PDMS as the substrate, we can clearly observe that the samples show a large relative resistance change even at smaller externally applied stresses (e.g. 5%, 10%). This judgment is also confirmed in the variation of their GF values. The GF value is a parameter used to visually measure the sensitivity, and its full name is the gauge factor. the GF is calculated as $\left[\frac{(R-R_0)}{R_0}\right]/\varepsilon$, where ε indicates the mechanical strain of the sample. In addition to the sensitivity, the response time and recovery time for the sample to respond to external changes are also important. **Fig. 2. (b)** shows the response time and the recovery time of the sample to a stress of 5 % at a velocity of 500 m/s. As can be seen from the figure, the response time (t_1) is about 520ms, and the recovery time (t_2) is about 69ms, which indicates that the response to the external tensile strain of the produced sample is relatively rapid and timely. Also, to demonstrate that the prepared PDMS-based LIG device has a preferable ohmic contact with the electrode, different voltages were applied to the sample under different stresses and the current changes were recorded, as in **Fig. 2. (c)**. In addition, the stability of the sensor under repeated external tensile-release strains also determines the quality of this sensor. **Fig. 2. (d)** shows the changing trend of the relative resistance change of the sample at 1 %, 2 %, 5 %, 10 %, and 15 %. It can be observed from the figure that when the external stress is in the range of 1 % - 15 %, the responses of the samples all show good stability. Since it is difficult to observe the relative change in resistance in the figure because the stress is small, **Fig. 2. (e)** is plotted separately to demonstrate the change in the relative resistance of the sample at 5 % repeated tensile-release cyclic strain. In order to prove that the sample has good long-term stability, the sample was strained at 10 % stress (this stress value has a large relative resistance change value, which is convenient to observe) for up to 8000 s of repeated stretch-release cycles as shown in **Fig. 2. (f)**, and a period was intercepted and plotted in **Fig. 2. (g)**, we can see that even during the long-term cycles, the

sample still maintains a relatively stable resistance (there is a drift of resistance change, but it is small and negligible), which is a good proof of the mechanical durability and long-term stability of the fabricated sample and reflects its superior performance. In addition, when printing LIG samples using different power levels and successfully transferring and testing their performance, it can be noticed in that the higher the power set, the lower the resistance value of the samples obtained. This result is plotted in **Fig. 2. (h)**.

3.3 The Acoustical Performance of the LIG devices

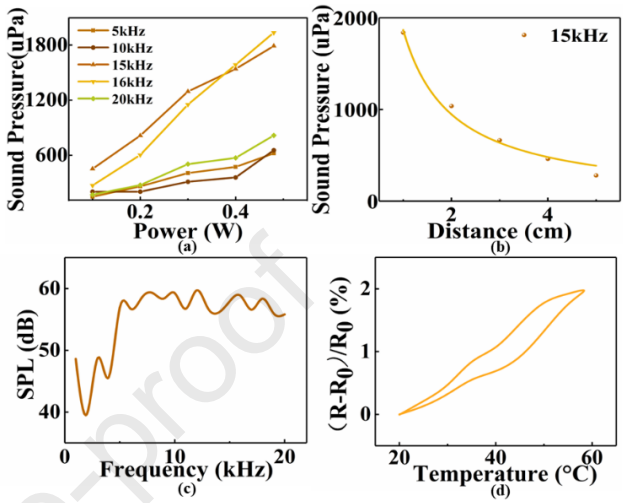

Fig. 3. The acoustical performance and the thermal sensitivity of the LIG sample. (a) the change of the output sound pressure (SP) of the sample under different applied power and frequency, keeping 1 cm. (b) The SP with the varied distance between the LIG device and the microphone, keeping 15 kHz. (c) The SPL of the fabricated sample with the sound frequency from 200 Hz to 20 kHz. (d) the resistance value of the sample in the heating and cooling cycle.

Keeping the distance between the sample and the microphone at 1 cm, the frequency is gradually increased from 5 kHz to 20 kHz, and the change of the output SP is recorded as in **Fig. 3. (a)**. We can observe that the output SP at any frequency tends to increase as the applied power increases, and the SPL

value is the largest when the frequency is close to 15 kHz or near 15 kHz. This indicates that the sound generation performance of the prepared LIG sensor gradually improves when the frequency of the applied AC sinusoidal voltage is gradually increased, which will provide some reference for the sensor design. Meanwhile, in order to investigate the relationship between distance and output SP, we varied the distance between the sample and the microphone and recorded the obtained data. It can be noticed in **Fig. 3. (b)** that the sound pressure gradually decreases as the distance increases, and the relationship between the two is inversely proportional. This experimental result better validates the equation：

$$P_{rms} = \frac{m_{air} \times f}{2\sqrt{2C_p T_0 r}} \dot{Q}_{air} \quad (1)$$

where P_{rms} is the root-mean-square sound pressure, m_{air} is the molecular weight of air, f is the frequency of the acoustic, C_p is the heat capacity under constant pressure, T_0 is the indoor temperature, r is the distance between the sound source with the microphone, and Q_{air} is the thermal energy diffused into the air.

Fig. 3. (c) plots the output sound pressure level (SPL) of the fabricated sample concerning the sound frequency from 200 Hz to 20 kHz. This curve is normalized by the input power (1 W). As can be seen from the figure, in the low-frequency band, the sample device emits a small sound, with the increase in the frequency of the sinusoidal AC voltage, the sound pressure level of the device gradually grows, and fluctuates in the middle and high-level band near a larger value, more stable.

3.4 The Thermal Sensitivity of the LIG Devices

The prepared samples were placed on the heating table, the heating time was set, the temperature of the heating table was gradually increased, and the changes in the resistance values of the samples under heating were recorded in real-time using a multimeter. The temperature of the heating table was gradually heated from room temperature to 20 °C to 60 °C, and the resistance value of the prepared LIG devices was seen to increase gradually, which may be due to the fact that the PDMS-based LIG

devices had a certain degree of deformation after heating, and the expansion of the devices resulted in the equivalent of a stretching effect on them, making the sample resistance value rise.

After holding the sample at 60 °C for a period of time, the temperature of the heating table was reset to room temperature to gradually cool it down, and the changes in the resistance value of the sample during the process of cooling down to the original temperature were recorded with a multimeter. It can be seen from **Fig. 3. (d)** that the resistance value of the sample gradually decreases during the cooling down process and returns to the original resistance value at 20 °C. This indicates that the resistance value of the PDMS as the sample is gradually decreasing. This indicates that the electrical properties of the proposed PDMS-based LIG device have good recoverability and can return to the original state after being subjected to external thermal disturbance.

3.5 The Application of the LIG Devices

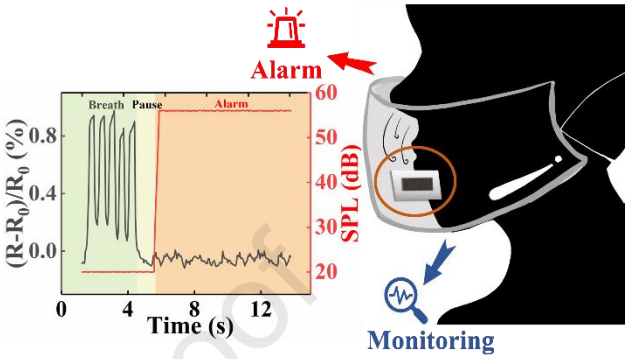

Fig. 4. When a respiratory pause exceeds a certain time, the operating mode of the device changes from monitoring to alarm, emitting an alarm sound close to 60 sound pressure level.

Based on the mechanical sensitivity and good acoustic performance of the LIG devices studied in the previous section, we can make an experimental verification of their application in wearable health monitoring electronic devices, which means health monitoring and alarm testing. The LIG device is set to operate in two modes: monitoring mode and alarm mode. Once a respiratory pause is detected for a certain period of time, the microcontroller control unit will give instructions to the signal generator to apply an AC voltage to the device to cause it to

sound an alarm, at which point the LIG device operates in alarm mode. Similarly, this function of the device can be used to monitor cardiac arrest, a life-threatening health problem, but it was not verified here due to the unworkability of the simulation experiment. The results of the experiment are shown in **Fig. 4**. First, a normal respiration check is performed, and when the respiratory pause exceeds a certain time, the device no longer undergoes a small deformation, and the microcontroller applies an 8 kHz AC voltage to the device to cause an alarm and record the SPL.

Therefore, this simulation experiment shows that the PDMS-based LIG devices can be applied to health monitoring wearable devices due to their mechanical sensitivity and good acoustic performance, and only limited assumptions have been made here.

4. Conclusions

In general, based on the structure and properties of laser-induced graphene (LIG) devices, PDMS is selected as its transfer substrate to obtain devices with high sensitivity, stable stretching properties, better-sounding properties, and excellent thermal stability. After experimental studies, the fabricated LIG devices can be successfully transferred when the printing power is 3.6 – 5.0 W and the printing speed is 100 mm/s. When the power is 5.0 W, the obtained LIG devices have relatively the highest mechanical properties; when the power is 5.0 W, the obtained LIG devices also have the best acoustic properties. As the laser power increases, the device exhibits better sensitivity and its sound generation performance is also better. But the higher the power, the more loose the device structure becomes, the more unstable the structure becomes, the more prone it is to fracture, and the strain it can withstand is smaller. Therefore , devices obtained by printing at appropriate laser power can be selected according to the application scenario to achieve the goal in practical applications. In addition, the LIG based on PDMS also has relatively good thermal sensitivity and thermal stability. Based on the above advantages of

LIG devices transferred to PDMS, they can combine mechanical sensing and sound generation in a single device, which is highly valuable for applications where sensing and timely warning are required. Such as respiratory pulse detection class wearable health detection devices, motion recognition, blind sign language to sound, etc. Therefore, due to the multi-parameter integration of the resulting device, it can provide new ideas for the invention and improvement of health detection-oriented sensing devices, portable electronic devices, and other objects.

CRediT authorship contribution statement

Lu-Qi Tao: Writing, Data analysis. **Chenwei Gao:** Visualization, Investigation. **Guanya Wang:** Supervision, Conceptualization, Methodology. **Hao Sun:** Investigation. **Liang-Yan Guo:** Writing, Reviewing, Editing. **Tian-Ling Ren:** Supervision.

Declaration of Competing Interest

The authors declare that they have no known competing financial interests or personal relationships that could have appeared to influence the work reported in this paper.

Acknowledgments: This work was supported by the National Natural Science Foundation of China (61901064), part by the China Postdoctoral Science Foundation（2022BG011）, in part by the Natural Science Foundation of Chongqing (cstc2020jcyj-msxmX0397), in part by the Chongqing Special Key Project for Technological Innovation and Application Development (cstc2019jscx-fxyd0262), in part by the Fundamental Research Funds for Central Universities (2020CDJ-LHZZ-077), and in part by the Fundamental Research Funds for Central Universities (00007717).

References

[1] D. Adeloye et al., The long-term sequelae of COVID-19: an international consensus on research priorities for patients with pre-existing and new-onset airways disease, Lancet Resp. Med. 9 (2021) 1467-1478.

[2] H.-R. Lim, H. S. Kim, R. Qazi, Y. T. Kwon, J. W. Jeong, and W. H. Yeo, Advanced Soft Materials, Sensor Integrations, and Applications of Wearable Flexible Hybrid Electronics in Healthcare, Energy, and Environment, Adv. Mater. 32 (2020) 1901924.1-1901924.43.

[3] D.Y. Park, D.J. Joe, D.H. Kim, H. Park, J.H. Han, C.K. Jeong, H. Park, J.G. Park, B. Joung, and K.J. Lee, Self-Powered Real-Time Arterial Pulse Monitoring Using Ultrathin Epidermal Piezoelectric Sensors, Adv. Mater. 29 (2017) 1702308.

[4] M. Mannoor, H. Tao, J. Clayton, et al., Graphene-based wireless bacteria detection on tooth enamel, Nat. Commun. 3 (2012) 763.

[5] S. P. Lee, G. Ha, D. E. Wright, Y. Ma, E. Sen-Gupta, N. R. Haubrich, P. C. Branche, W. Li, G. L. Huppert, M. Johnson, H. B. Mutlu, K. Li, N. Sheth, J. A. Wright, Y. Huang, M. Mansour, J. A. Rogers, and R. Ghaffari, Highly flexible, wearable, and disposable cardiac biosensors for remote and ambulatory monitoring, npj Digital. Med.1 (2018) 2.

[6] L. Wang, Y. Li, et al., Weaving Sensing Fibers into Electrochemical Fabric for Real‐Time Health Monitoring, *Adv.* Funct. Mater. 28 (2017) 1804456.1-1804456.8.

[7] X. Chen et al., A Dual‐Functional Graphene‐Based Self‐Alarm Health‐Monitoring E‐Skin, Adv. Funct. Mater. 29 (2019) 1904706.1-1904706.9.

[8] B. Sun, R. N. McCay, S. Goswami, Y. Xu, C. Zhang, Y. Ling, J. Lin, Z. Yan, Gas‐permeable, multifunctional on‐skin electronics based on laser‐induced porous graphene and sugar‐templated elastomer sponges, Adv. Mater. 30 (2018) 1804327.

[9] G. Wang, L.-Q. Tao, Z. Peng, et al., Nomex paper-based double-sided laser-induced graphene for multifunctional human-machine interface, Carbon, 193 (2022) 68-76.

[10] L. Huang, H. Wang, D. Zhan and F. Fang, Flexible Capacitive Pressure Sensor Based on Laser–Induced Graphene and Polydimethylsiloxane Foam, IEEE Sensors J. 21 (2021) 12048-12056.

[11] X. Chen, D. Zhang, H. Luan, et al. Flexible Pressure Sensors Based on Molybdenum Disulfide/ Hydroxyethyl Cellulose/Polyurethane Sponge for

Motion Detection and Speech Recognition Using Machine Learning. ACS applied materials & Interfaces, 15(2022) 2043-2053.

[12] H. Zhang, D. Zhang, B. Zhang, D. Wang, M. Tang. Wearable Pressure Sensor Array with Layer-by-Layer Assembled MXene Nanosheets/Ag Nanoflowers for Motion Monitoring and Human-Machine Interfaces. ACS Appl Mater Interfaces, 14(2022)48907-48916.

[13] W. Zhao, D. Zhang, Y. Yang, et al. A fast self-healing multifunctional polyvinyl alcohol nano-organic composite hydrogel as a building block for highly sensitive strain/pressure sensors. Journal of Materials Chemistry A, 9(2021)22082-22094.

[14] H. K. Ji, M. K. Ji, G. W. Lee, et al., Advanced Boiling-A Scalable Strategy for Self-Assembled Three-Dimensional Graphene, ACS Nano, 12 (2021) 2839−2848.

[15] X. Zhao, Y. Long, T. Yang, J. Li, and H. Zhu, Simultaneous High Sensitivity Sensing of Temperature and Humidity with Graphene Woven Fabrics, ACS Appl. Mater. Interfaces, 9 (2017) 30171−3017.

[16] K. Chen, L. Shi, Y. Zhang, Z. Liu, et al., Scalable chemical-vapor-deposition growth of three-dimensional graphene materials towards energy-related applications, Chem. Soc. Rev. 47 (2018) 3018.

[17] J. Sha, C. Gao, S.-K. Lee, Y. Li, N. Zhao, and J. M. Tour, Preparation of Three-Dimensional Graphene Foams Using Powder Metallurgy Templates, ACS Nano, 10 (2016) 1411.

[18] X. Yang, C. Cheng, Y. Wang, L. Qiu, and D. Li, Liquid-Mediated Dense Integration of Graphene Materials for Compact Capacitive Energy Storage, Science, 34 (2013) 534-537.

[19] V. Chabot, D. Higgins, A. Yu, X. Xiao, Z. Chen, and J. Zhang, A review of graphene and graphene oxide sponge: material synthesis and applications to energy and the environment, Energ. Environ. Sci. 7 (2014) 1564-1596.

[20] Y. Zhou et al., Preparation methods and development and application prospects of graphene, Ordnance Mater. Sci. Eng. 35 (2012) 86-90.

[21] J. Lin, Z. Peng, Y. Liu, F. Ruiz-Zepeda, R. Ye, E. L. G. Samuel, M. J. Yacaman, B. I. Yakobson, and J. M. Tour, Laser-induced porous graphene films from

commercial polymers, Nat. Commun. 5 (2014).

[22] Y. Huang, L.-Q. Tao, J. Yu, Z. Wang, and X. Chen, Integrated Sensing and Warning Multifunctional Devices Based on the Combined Mechanical and Thermal Effect of Porous Graphene, ACS Appl. Mater. Interfaces, 12 (2020) 3049-53057.

[23] R. Ye, D. K. James, and J. M. Tour, Laser-induced graphene, Acc. Chem. Res. 51 (2018) 1609-1620.

[24] B. Sindhu, A. Kothuru, P. Sahatiya, S. Goel and S. Nandi, Laser-Induced Graphene Printed Wearable Flexible Antenna-Based Strain Sensor for Wireless Human Motion Monitoring, IEEE Trans. Electron Devices, 68 (2021) 3189-3194.

[25] S. Zou, L.-Q. Tao, G. Wang, et al., Humidity-Based Human–Machine Interaction System for Healthcare Applications, ACS Appl. Mater. Interfaces, 14 (2022) 12606-12616.

[26] A. Kaidarova and J. Kosel, Physical Sensors Based on Laser-Induced Graphene: A Review, IEEE Sensors J. 21 (2021) 12426-12443.

[27] H. Sun, L.-Q. Tao, P. Wang, et al., A flexible graphene-based fabric ultrasound source for machine learning enhanced information encryption, IEEE Electron Device Lett (2022).

[28] B. Demelash Abera et al., Laser-fabricated flexible nanographene-based sensor for pH detection in saliva, IEEE Sensors J. (2020) 1-4.

[29] L. Huang, H. Wang, D. Zhan and F. Fang, Flexible Capacitive Pressure Sensor Based on Laser–Induced Graphene and Polydimethylsiloxane Foam, IEEE Sensors J. 21 (2021) 12048-12056.

[30] M. Nie, Yh. Xia, and Hs. Yang, A flexible and highly sensitive graphene-based strain sensor for structural health monitoring, Cluster Comput. 22 (2019) 8217–8224.

[31] G. Wang, L.-Q. Tao, T. Li, et al. High-performance flexible heater with command-responding function attained by direct laser writing on Nomex paper, IEEE Electron Device Lett. 43 (2022) 462-465.

Lu-Qi Tao: Writing, Data analysis. **Chenwei Gao:** Visualization, Investigation. **Guanya Wang:** Supervision, Conceptualization, Methodology. **Hao Sun:** Investigation. **Liang-Yan Guo:** Writing, Reviewing, Editing. **Tian-Ling Ren:** Supervision.

Declaration of interests

☒ The authors declare that they have no known competing financial interests or personal relationships that could have appeared to influence the work reported in this paper.

☐The authors declare the following financial interests/personal relationships which may be considered as potential competing interests: